

Entanglement induced by Heisenberg exchange between an electron in a nested quantum dot and a qubit with relative motion

Lee-Che Lin,¹ Seng Ghee Tan,² Ching-Ray Chang,³ Shih-Jye Sun,⁴ and Son-Hsien Chen^{1,*}

¹*Department of Applied Physics and Chemistry, University of Taipei, Taipei 10048, Taiwan*

²*Department of Optoelectric Physics, Chinese Culture University, Taipei 11114, Taiwan*

³*Quantum Information Center, Chung Yuan Christian University, Taoyuan, 320314, Taiwan*

⁴*Department of Applied Physics, National University of Kaohsiung, Kaohsiung 81148, Taiwan*

(Dated: December 14, 2024)

We propose a nested quantum dot structure for improved control of entanglement induced by the Heisenberg exchange between an electron and a qubit with relative motion. The entanglement is quantified by the mutual information (MI). The electron, initially prepared in the ground state, generally produces greater entanglement when excited to the scattering state compared to remaining in the bound state. In the bound state, the final entanglement oscillates as a function of the qubit speed and can be tuned accordingly. In the case of long-range interaction, the normalized exchange distribution leads to substantial final entanglement, independent of the qubit moving direction, indicating that even very weak but prolonged exchange can still generate significant entanglement. In the case of short-range interaction, different moving directions lead to varying MI values. We also consider the scenario without the nested dot and find that the same maximum (among all times) MI is pre-determined solely by the initial angle between the spins. In this case, the entanglement exhibits different growth characteristics during different phases. The saturation of the MI mimics that of a strict zero-dimensional quantum dot, where exchange and time are combined into a single parameter, the amount of interaction.

I. INTRODUCTION

Quantum entanglement represents a profound phenomenon in quantum mechanics, where two or more subsystems are intrinsically correlated such that the quantum state of each subsystem cannot be described independently [1, 2]. Comprehending how entanglement is built [3] is crucial for advancing both theoretical understanding and technological applications [2, 4–16] in quantum systems. One salient mechanism of generating entanglement is through the spin-spin exchange interaction of the form $\Gamma_{\alpha\beta}S_{\alpha}S_{\beta}$, where S_{α} and S_{β} represent the spin operators along the α and β directions ($\alpha, \beta \in \{x, y, z\}$), respectively. The Heisenberg exchange [17], contributes through the diagonal elements of the matrix Γ , while the Dzyaloshinsky-Moriya exchange [18, 19] appears through the off-diagonal elements; the Kaplan-Shekhtman-Entin-Wohlman-Aharony exchange [20, 21], manifests through both diagonal and off-diagonal elements [22, 23]. Among these exchanges, the Heisenberg exchange stands out, as it does not require spin-orbit interactions and demonstrates an entanglement phase transition in thermal states [24]. The critical temperature for this transition can be controlled through the exchange anisotropy and the external magnetic field [24, 25]. Furthermore, even weakly entangled states have been shown to be useful for achieving high-precision measurements [26]. The randomization of Heisenberg exchange [27] enables highly accurate magnetic field detection by measuring the state return probability [28].

The minimal set required to form entanglement is a two-qubit system. Particularly, the electron spin-qubit state in quantum dots (QDs) [29–32] has been experimentally realized, with the Heisenberg exchange interaction coupling between the qubits [33–35]. This minimal set exhibits exotic dynamics. For instance, when two qubits interact with a common environment, their entanglement can abruptly disappear [36–43] more easily than in systems beyond the minimal set. By applying an exponentially time-varying magnetic field, the final entanglement between the two qubits can be effectively preserved [44]. Additionally, in a closed two-qubit system, the evolved states span two separate Hilbert subspaces in the presence of a time-varying nonuniform magnetic field [45].

Moreover, entanglement becomes more amendable by permitting qubits to move freely in space. By tuning the velocities of two atom qubits moving within their respective cavities, which act as interacting local environments, the initial entanglement can be maintained [46]. For spin qubits, properly assigning the interaction time during which a qubit sequentially interacts with all others, a generalized W-state [47] is achievable [48]. In addition, when sending qubits to scatter off static qubits via local Heisenberg exchange, the transmission coefficients of the scattered qubits can be analyzed to yield tomography of the static spin qubits, enabling the reconstruction of their quantum states [49]. Robust entanglement between two ballistic electrons can be built from scattering off a magnetic impurity [50]. However, few studies have investigated how the interplay among confinement potential, exchange strength, interaction duration, and initial qubit configurations affects entanglement. It remains unclear which of these factors primarily determines the final entanglement.

* sonhsien@utapei.edu.tw

In this paper, we examine the entanglement in a closed system consisting of an electron and a qubit with relative speed in the nonrelativistic regime. The qubit entangles with the electron via Heisenberg exchange. The electron is confined in a quasi zero-dimensional (0D) QD, namely of finite size in the x -direction. We find that the exchange interaction duration and strength play a similar role in establishing and fine-tuning the entanglement, whose maximum value is pre-set by the initial spin angle between the electron and the qubit. A nested quantum dot (NQD) is introduced to control the electron state, either bound or scattering, each exhibiting distinct entanglement behaviors. Accordingly, the proposed nested dot structure permits entanglement to be adjusted electrically. Furthermore, the similarity between the mechanisms of interaction duration and strength offers a fresh perspective on describing and manipulating entanglement dynamics.

The paper is organized as follows. In Sec. II, we introduce the system under study and address the mutual information (MI) [51, 52], which serves as the entanglement monotone employed in this work. Our numerical simulations are presented and discussed in Sec. III for the QD (Sec. III A) and NQD (Sec. III B) systems. Section IV concludes our findings.

II. MODELS AND METHODS

We consider the Hamiltonian that captures relative motion between the electron and the qubit as

$$H(t) = \sum_i V_g(x_i) c_i^\dagger c_i - \gamma \sum_{\langle ij \rangle} c_i^\dagger c_j + \sum_{i,ss's''s'''} J(x_i,t) \times c_{is}^\dagger c_{is'} d_{s''}^\dagger d_{s'''} (\vec{\sigma}^e)_{ss'} \cdot (\vec{\sigma}^q)_{s''s'''} \quad (1)$$

Here c_{is}^\dagger (c_{js}) denotes the creation (annihilation) operator that creates (annihilates) an electron with spin $s = \uparrow, \downarrow$ on site i . The operators d_s^\dagger and d_s represent the creation and annihilation of the qubit, respectively; the $\vec{\sigma}^e$ are the Pauli spin matrices of the electron, and $\vec{\sigma}^q$ the spin matrices of the qubit. The kinetic energy is characterized by the hopping γ between two nearest-neighbor sites $\langle ij \rangle$. An infinite quantum well confines the electron within $x_{i=1}$ to $x_{i=N}$, as shown in Fig. 1(a). Further applying the gate voltage potential $V_g(x_i)$ produces a nested dot structure, as depicted in Figs. 2(a) and 3(a). The velocity of the moving qubit is introduced through the time-dependent exchange coupling $J(x_i, t)$.

Specifically, in the scenario of a qubit moving at constant velocity \vec{v}^q , Figs. 2(a) and 3(a), we assign

$$J(x_i, t) = \frac{J_0}{\sqrt{\pi}w_J} \exp\left(-\frac{|\vec{r} - \vec{v}^q(t-t_0)|^2}{w_J}\right). \quad (2)$$

The electron wave function $|\psi^e(x_i, t)\rangle$ varies with the position vector $\vec{r} = (x_i - x_0, y = 0)$ and is confined initially

inside the NQD. The NQD centered at x_0 is subject to $V_g(x_i)$. The effective exchange distribution experienced by the electron is assumed to follow a Gaussian form, normalized by the prefactor $1/\sqrt{w_J}$. This normalization allows entanglements in different interaction ranges w_J to be compared on an equal footing. We let the qubit pass over the dot center x_0 at time t_0 , at which the maximum exchange takes place. On the other hand, in the scenario of a static qubit located at x_{i^*} [Fig. 1(a)] we adopt the local exchange,

$$J(x_i, t) = J_0 \delta_{i,i^*}. \quad (3)$$

The studied quasi-0D system can be carried out using gate-defined quantum dots [31]. Especially, exchange with the moving qubit is achievable in solid-state systems [53] such as a single-walled carbon nanotube [54].

The total wave function in the closed system evolves according to the Schrodinger equation,

$$i \frac{\partial}{\partial t} |\Psi(x_i, t)\rangle = H(t) |\Psi(x_i, t)\rangle, \quad (4)$$

(reduced Planck constant $\hbar \equiv 1$) with the separable initial conditions (ICs),

$$|\Psi(x_i, 0)\rangle = |\psi^e(x_i, 0)\rangle \otimes |\chi^e\rangle \otimes |\chi^q\rangle \quad (5)$$

where $|\chi^e\rangle$ and $|\chi^q\rangle$ are the spin sates of the electron and qubit, respectively. The system is in a pure state described by the density matrix (DM) $\rho(x_i, x_j, t) = |\Psi(x_i, t)\rangle \langle \Psi(x_j, t)|$. The MI [51, 52]

$$\mathcal{M}(\rho) = \mathcal{S}(\rho^e) + \mathcal{S}(\rho^q) - \mathcal{S}(\rho)$$

detects quantum entanglements via the Von Neumann entropy $\mathcal{S}(\rho^{e/q}) = -Tr(\rho^{e/q} \ln \rho^{e/q})$. Here $\rho^{e/q} = Tr_{q/e}(\rho^{e/q})$ is the reduced DM of the corresponding subsystems. Since the system state is pure, $\mathcal{S}(\rho) = 0$, the correlations detected by the MI correspond to quantum correlations rather than classical correlations.

III. NUMERICAL SIMULATION AND DISCUSSION

Regard the total *amount of interaction* characterized by,

$$\int_{-\infty}^{\infty} J^e(t) dt, \quad (6)$$

where $J^e(t) = \sum_{i=1}^N |\psi^e(x_i, t)|^2 J(x_i, t)$ quantifies the exchange electron experienced at time t . Three scenarios are considered. In the first scenario Fig. 1, the electron is injected into the QD, allowing for an *infinite* amount of interaction. In the second (third) scenario Fig. 2 (Fig. 3), the qubit moves longitudinally (transversely) through the NQD, generating a *finite* amount of interaction.

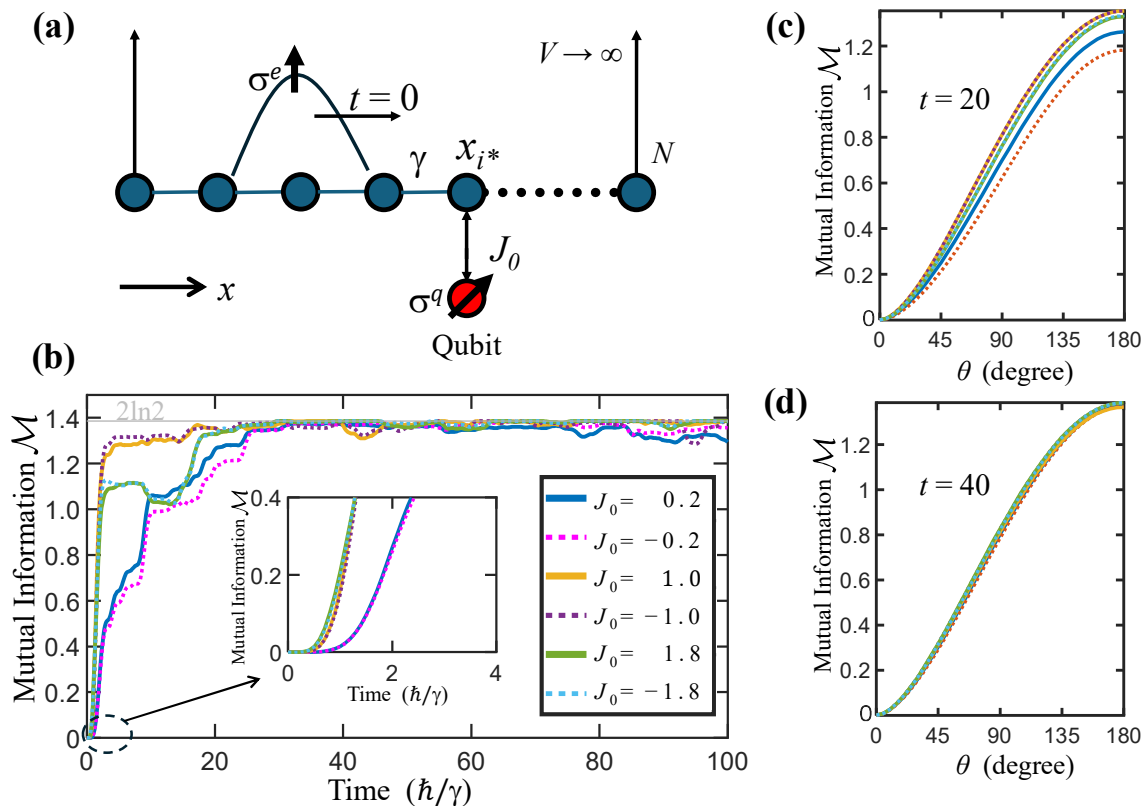


FIG. 1. (a) Schematic of a right-moving electron wave packet initially centered at $x_c = 12a$, which will interact, via Heisenberg exchange J_0 , with the qubit of fixed position at $x_{i^*} = 16a$; a is the lattice spacing. The quantum dot is quasi 0D of finite size with $i = 1, 2, \dots, N = 21$ lattice points formed by an infinite potential well ($V = \infty$ outside the dot). The initial angle between the electron spin $\vec{\sigma}^e$ and the qubit $\vec{\sigma}^q$ is θ . (b) Mutual information at $\theta = \pi$ as a function of time t for different values of J_0 . The inset provides a zoomed view around $t \approx 0$. (c) and (d) the mutual information as a function of θ at $t = 20$ and $t = 40$ for various values of J_0 , respectively.

In what follows, we present our numerical results using (4) for a QD containing $N = 21$ sites. Exchange J and potential V_g energy are in units of γ , and time t is in unit of \hbar/γ . The relative motion is modeled by either a moving electron or a moving qubit. Both cases employ an infinite quantum well. However, in the latter, a sub-well by V_g confines the electron initially in its ground state, after which the electron is excited by the itinerant qubit that effectively provides a finite interaction as the exchange decays in the long-time limit. The former, on the other hand, produces a permanent exchange with the qubit that resides at a fixed position x_{i^*} inside the dot.

A. Electron injected into a quantum dot

Consider an electron injected from the left to the localized qubit, Fig. 1. The IC of the electron is described

by the Gaussian wave packet,

$$\psi^e(x_i, 0) = \frac{1}{\sqrt{C}} \exp\left(-\frac{(x_i - x_c)^2}{2} + ik(x_i - x_c)\right),$$

in Eq. (5). Here for right-moving electron propagation, we set positive $k = 1$, and C is a constant assigned according to the probability normalization, $\sum_{i=1}^N |\psi^e(x_i, 0)|^2 = 1$. The initial peak of the Gaussian $x_c = 12$ of the electron and the qubit position $x_{i^*} = 16$ (in unit of lattice spacing a) generating local exchange (3) are adopted; θ denotes the angle between the spins $|\chi^e\rangle$ and $|\chi^q\rangle$. Since the local exchange felt by the electron does not decay over time, the amount of interaction is infinite.

As shown in Fig. 1(b), rapidly growing entanglement is observed immediately after the electron wave function arrives at the site x_{i^*} . Following this growth phase, MI develops slowly and is modulated by the back-and-forth

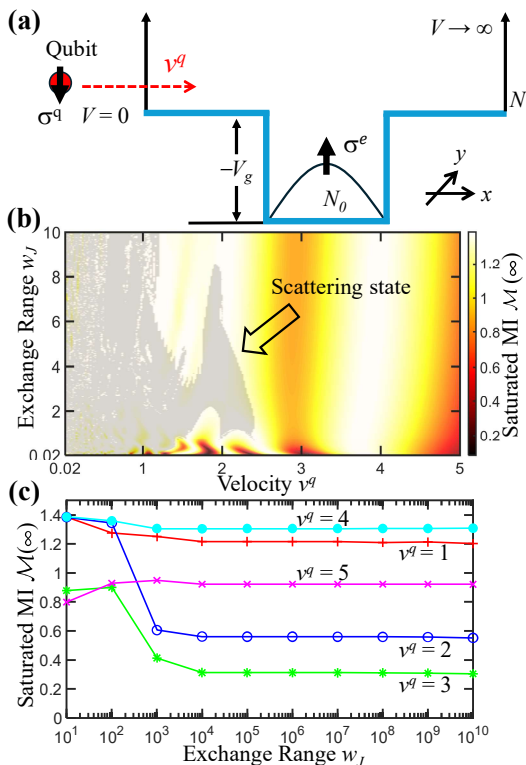


FIG. 2. (a) Schematic of a qubit moving longitudinally along the x -direction at a constant speed v^q through a nested quantum dot of size N_0 and applied gate voltage potential $-V_g$. The electron is prepared in the ground state, confined within the nested dot, and experiences the effective exchange Eq. (7) due to the moving qubit. (b) Saturated mutual information $\mathcal{M}(t \rightarrow \infty)$ as a function of the exchange range w_J and speed v^q . The shaded region indicates where the electron becomes excited out of the nested dot, transitioning to a scattering state. (c) Logarithmic plot of the w_J dependence of the saturated mutual information at various v^q .

scattering of the electron bouncing off the infinite potential well. A certain maximum MI \mathcal{M}_{\max} is then reached, and the system tends to build a saturation of MI eventually. In the early stage, as shown in Fig. 1(c), different exchange values J_0 yield different MI. However, as the system evolves further, Fig. 1(d), the MI follow a behavior that can be fit by $[1 - \cos(\theta)] \times \ln 2$ and becomes insensitive to J_0 as well as the coupling type, whether ferromagnetic $J_0 < 0$ or antiferromagnetic $J_0 > 0$. These saturation ($t \gg 0$) features are similar to those of the strict 0D case $N = 1$ [43], where exchange J_0 and time t play the same role by entering the dynamics through a single variable $J_0 \times t$ as Eq. (6) suggests. Interestingly, we observe that \mathcal{M}_{\max} depends only on the initial angle θ . In other words, the maximum entanglement is intrinsically

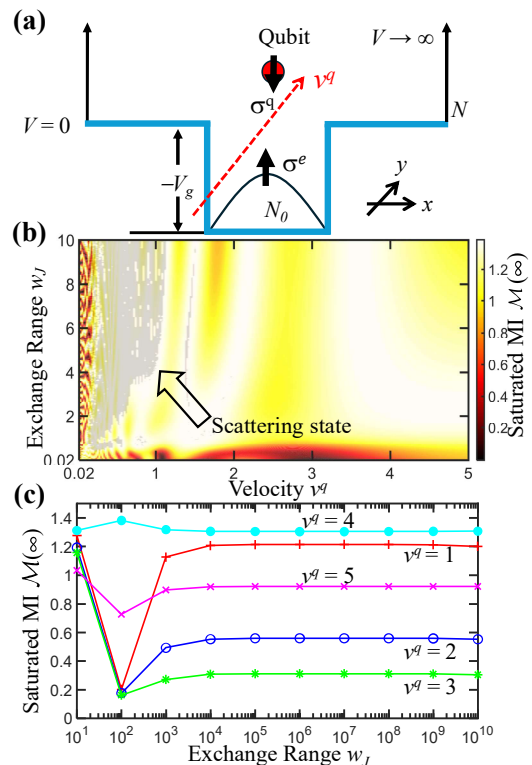


FIG. 3. (a) Schematic of the nested quantum dot similar to Fig. 2 but with the qubit moving transversely along y -direction, described by the exchange, Eq. (8). (b) Saturated mutual information $\mathcal{M}(t \rightarrow \infty)$ as a function of the exchange range w_J and speed v^q . The shaded region indicates the scattering states. (c) Saturated $\mathcal{M}(t \rightarrow \infty)$ as a function of the logarithmic scale of w_J for different values of v^q . Note that this represents the scenario with the weakest amount of electron-qubit interaction among all the device structures proposed herein.

pre-set (before interaction takes place) by $\mathcal{M}_{\max}(\theta)$; the initial angle becomes the sole relevant factor limiting the maximum possible entanglement that can be established, overriding interaction strength, dot size, and initial electron speed and distribution. In fact, we find that the same θ -determined maximum $\mathcal{M}_{\max}(\theta)$ from the infinite-amount interaction also defines the maximum entanglement from the finite-amount interaction due to a moving qubit initially at the same θ . We discuss the scenario of a moving qubit below.

B. Qubit moving through a nested quantum dot

Consider now the qubit moving at a constant speed v^q . As aforementioned, the maximum is set by \mathcal{M}_{\max} . We choose the anti-parallel configuration $\theta = \pi$, for which $\mathcal{M}_{\max} = 2 \ln 2 \approx 1.386$ [refer also to Fig. 1(d)]. Accordingly to Eq. (2), when the qubit moves longitudinally along the x -direction in Fig. 2(a), one has $\vec{v}^q = (v^q, 0)$ leading to

$$J(x_i, t) = \frac{J_0}{\sqrt{\pi w_J}} \exp\left(-\frac{[(x_i - x_0) + v^q(t - t_0)]^2}{w_J}\right), \quad (7)$$

in the Hamiltonian (1). When the qubit moves transversely along the y -direction in Fig. 3(a), one has $\vec{v}^q = (0, v^q)$ resulting in

$$J(x_i, t) = \frac{J_0}{\sqrt{\pi w_J}} \exp\left(-\frac{(x_i - x_0)^2}{w_J}\right) \times \exp\left(-\frac{(v^q)^2(t - t_0)^2}{w_J}\right). \quad (8)$$

For a given v^q , the exchange (8) represents the case with the weakest amount of interaction among all scenarios studied herein. In the QD, an inner area is subject to a voltage potential $-V_g(x_{i=8,9,\dots,14}) = -0.4$, forming a NQD of size $N_0 = 7$. The selected V_g produces 10 bound states in the NQD, and the electron is correspondingly prepared in the lowest energy state. We set exchange $J_0 = 5$, so that the electron initially trapped in the nested dot can be excited to the scattering state (i.e., outside the NQD) when the amount of interaction is enough. The qubit is initially assumed to be outside the dot and far from the electron by assigning a sufficiently large $t_0 = 1500$. At time t_0 , the qubit arrives at the center of the NQD and then starts to move away from the dot.

The final MI $\mathcal{M}(t \rightarrow \infty)$ as a function of the interaction range w_J and the qubit speed v^q is shown in Fig. 2(b) for the longitudinal motion and in Fig. 3(b) for the transverse motion. The shaded region signifies the state where the electron is scattered outside the NQD. Note that the additional term $J_0/\sqrt{\pi w_J} \exp[-2v^q(x_i - x_0)(t - t_0)/w_J]$, as seen by comparing Eqs. (7) and (8), accounts for the longer interaction duration in the case of longitudinal motion. Therefore, for a given v^q , to achieve the same amount of interaction necessary for the electron to be excited to the scattering state, the transverse case requires a longer exchange range w_J . In the transverse case, but not the longitudinal case, our results indicate that when the qubit moves very slowly, the final MI alternates and exhibits high sensitivity to w_J . For a given w_J , in both cases, however, a smaller v^q (and thus a longer duration) does not always lead to a larger saturated MI. In fact, the saturated MI oscillates with v^q . In the limit of very fast speed v^q and very short range w_J , MI decays to zero due to extremely small interaction duration. Nonetheless, a

feature independent of the moving direction, the range w_J , and the speed v^q , is that the scattering states generally yield larger saturated entanglement than bound states.

The benefit to introduce the NQD then emerges. The device is multi-functional, allowing both scattering and bound states to be utilized for different purposes. If larger entanglement is desired, the scattering state is preferable. If tunability of the final entanglement is required, bound states can be exploited by adjusting the speed v^q .

Figures 2(c) and 3(c) illustrate how the final MI $\mathcal{M}(t \rightarrow \infty)$ varies with increasing w_J for longitudinal and transverse motion, respectively. We note that the qubit eventually interacts effectively with a single-electron QD of zero size due to their large separation distance, regardless of the moving direction of \vec{v}^q . However, for mild $w_J \lesssim N^2$, the final entanglement retains a memory of the \vec{v}^q direction and finite NQD size experienced around $t \approx t_0$. This can be seen by comparing $\mathcal{M}(t \rightarrow \infty)$ in Fig. 2(c) and in Fig. 3(c) for w_J less than 10^3 . Conversely, for long-range interaction, $w_J \gg N^2$, the memory effect of the moving direction is lost, i.e., both longitudinal and transverse \vec{v}^q yield the same $\mathcal{M}(t \rightarrow \infty)$. This loss suggests that the spatial information of the qubit (or spatial dependence of the exchange) is absent. Being worth noticing, even in the uniform limit of the exchange distribution, which leads to very weak but long-lasting interaction, significant entanglement can still be established, as indicated by the converged \mathcal{M} as $w_J \rightarrow \infty$.

IV. CONCLUSION

In conclusion, we explore the closed-system entanglement dynamics between an electron confined in an infinite quantum well (QD) and a qubit with relative motion. The Heisenberg exchange between the two spins induces entanglement. When the qubit is embedded in the dot, a moving electron described by an initial Gaussian wave packet yields permanent interaction. In this case, the total amount of interaction (6) is infinite, and the maximum (among all times) MI \mathcal{M}_{\max} , is pre-set solely by the initial spin angle θ . A rapid growth phase of entanglement is observed as the electron wave function reaches the site coupled to the qubit. This is followed by a slower growth during the near-saturation phase, where the electron undergoes back-and-forth scattering within the well. The saturation (set also by \mathcal{M}_{\max}) being independent of the exchange, resembles that of the strict 0D QD, where the amount $\int_{-\infty}^t J^e(t') dt'$ simplifies to $J_0 \times t$, determining the system evolution and effectively equating the roles of the exchange and time.

The same $\mathcal{M}_{\max}(\theta)$ also governs the maximum MI in the case of a finite amount of interaction, considering a moving qubit passing through the NQD, with the initial

electron in the ground state. The nested structure enables versatile control of the final entanglement. When the qubit moves slowly and the exchange strength is large, the electron can be excited to the scattering states (with a sufficient amount of interaction), thus achieving large entanglement. On the other hand, in the high-speed regime, where the electron remains in the bound state, the qubit speed can be used to adjust the final entanglement. For short-range exchange interactions, longitudinal and transverse motion lead to different final entanglement. Interestingly, for long-range exchange interactions, the final entanglement becomes insensitive to the moving directions. Even with a uniform distribution of the exchange, substantial MI can be obtained. Our findings across all scenarios suggest that weak but long-lasting exchange interactions can yield a considerable amount

of entanglement, with the primary bottleneck limiting the entanglement being the initial angle between the two spins. The proposed NQD offers a pathway for manipulating entanglement, while the identified features deepen our understanding of how the interaction duration, controlled by the relative motion between qubits, governs entanglement.

ACKNOWLEDGMENTS

One of the authors, S.-H. C., expresses gratitude to Ming-Chien Hsu and Che-Chun Huang for their valuable discussions. S.-G. Tan and C.-R. Chang acknowledge support from the National Science and Technology Council of Taiwan under Grant Nos. NSTC 113-2112-M-034-002 and NSTC 113-2112-M-033-011, respectively.

-
- [1] K. Życzkowski, P. Horodecki, M. Horodecki, and R. Horodecki, *Phys. Rev. A* **65**, 012101 (2001), URL <https://link.aps.org/doi/10.1103/PhysRevA.65.012101>.
- [2] R. Horodecki, P. Horodecki, M. Horodecki, and K. Horodecki, *Rev. Mod. Phys.* **81**, 865 (2009), URL <https://link.aps.org/doi/10.1103/RevModPhys.81.865>.
- [3] A. Nahum, J. Ruhman, S. Vijay, and J. Haah, *Phys. Rev. X* **7**, 031016 (2017), URL <https://link.aps.org/doi/10.1103/PhysRevX.7.031016>.
- [4] F. Y. Khalili and E. S. Polzik, *Phys. Rev. Lett.* **121**, 031101 (2018), URL <https://link.aps.org/doi/10.1103/PhysRevLett.121.031101>.
- [5] E. Zeuthen, E. S. Polzik, and F. Y. Khalili, *Physical Review D* **100**, 062004 (2019).
- [6] A. K. Ekert, *Physical review letters* **67**, 661 (1991).
- [7] P. W. Shor and J. Preskill, *Physical review letters* **85**, 441 (2000).
- [8] N. Gisin, G. Ribordy, W. Tittel, and H. Zbinden, *Reviews of modern physics* **74**, 145 (2002).
- [9] C. H. Bennett, *Physica Scripta* **1998**, 210 (1998).
- [10] D. P. DiVincenzo, *Science* **270**, 255 (1995).
- [11] A. Steane, *Reports on Progress in Physics* **61**, 117 (1998).
- [12] D. P. DiVincenzo, *Fortschritte der Physik: Progress of Physics* **48**, 771 (2000).
- [13] T. D. Ladd, F. Jelezko, R. Laflamme, Y. Nakamura, C. Monroe, and J. L. O'Brien, *nature* **464**, 45 (2010).
- [14] M. A. Nielsen and I. L. Chuang, *Quantum computation and quantum information* (Cambridge university press, 2010).
- [15] C. H. Bennett and D. P. DiVincenzo, *nature* **404**, 247 (2000).
- [16] L. S. Madsen, F. Laudenbach, M. F. Askarani, F. Rortais, T. Vincent, J. F. Bulmer, F. M. Miatto, L. Neuhaus, L. G. Helt, M. J. Collins, et al., *Nature* **606**, 75 (2022).
- [17] L. Amico, R. Fazio, A. Osterloh, and V. Vedral, *Rev. Mod. Phys.* **80**, 517 (2008), URL <https://link.aps.org/doi/10.1103/RevModPhys.80.517>.
- [18] T. Moriya, *Phys. Rev.* **120**, 91 (1960), URL <https://link.aps.org/doi/10.1103/PhysRev.120.91>.
- [19] T. Moriya, *Phys. Rev. Lett.* **4**, 228 (1960), URL <https://link.aps.org/doi/10.1103/PhysRevLett.4.228>.
- [20] T. Kaplan, *Zeitschrift für Physik B Condensed Matter* **49**, 313 (1983).
- [21] L. Shekhtman, O. Entin-Wohlman, and A. Aharony, *Phys. Rev. Lett.* **69**, 836 (1992), URL <https://link.aps.org/doi/10.1103/PhysRevLett.69.836>.
- [22] R. Citro and E. Orignac, *Phys. Rev. B* **65**, 134413 (2002), URL <https://link.aps.org/doi/10.1103/PhysRevB.65.134413>.
- [23] M. A. Yurischev, *Quantum Information Processing* **19**, 336 (2020).
- [24] X. Wang, *Phys. Rev. A* **64**, 012313 (2001), URL <https://link.aps.org/doi/10.1103/PhysRevA.64.012313>.
- [25] V. Azimi-Mousolou, A. Bergman, A. Delin, O. Eriksson, M. Pereiro, D. Thonig, and E. Sjöqvist, *Physical Review A* **106**, 032407 (2022).
- [26] R. Trényi, Á. Lukács, P. Horodecki, R. Horodecki, T. Vértesi, and G. Tóth, *New Journal of Physics* **26**, 023034 (2024).
- [27] S. Oh, Y.-P. Shim, J. Fei, M. Friesen, and X. Hu, *Phys. Rev. B* **85**, 224418 (2012), URL <https://link.aps.org/doi/10.1103/PhysRevB.85.224418>.
- [28] G. Biswas, S. Sengupta, and A. Biswas, *arXiv preprint arXiv:2410.22723* (2024).
- [29] M. Veldhorst, C. Yang, J. Hwang, W. Huang, J. Dehollain, J. Muhonen, S. Simmons, A. Laucht, F. Hudson, K. M. Itoh, et al., *Nature* **526**, 410 (2015).
- [30] Y. P. Kandel, H. Qiao, S. Fallahi, G. C. Gardner, M. J. Manfra, and J. M. Nichol, *Nature* **573**, 553 (2019).
- [31] C. J. van Diepen, T.-K. Hsiao, U. Mukhopadhyay, C. Reichl, W. Wegscheider, and L. M. Vandersypen, *Physical Review X* **11**, 041025 (2021).
- [32] J. Abouie and D. Vashaee, *Advanced Quantum Technologies* **7**, 2400117 (2024).
- [33] A. Johnson, J. Petta, J. Taylor, A. Yacoby, M. Lukin, C. Marcus, M. Hanson, and A. Gossard, *Nature* **435**, 925 (2005).
- [34] F. H. Koppens, J. A. Folk, J. M. Elzerman, R. Hanson, L. W. Van Beveren, I. T. Vink, H.-P. Tranitz, W. Wegscheider, L. P. Kouwenhoven, and L. M. Vandersypen, *Science* **309**, 1346 (2005).
- [35] J. Petta, A. Johnson, J. Taylor, A. Yacoby, M. Lukin,

- C. Marcus, M. Hanson, and A. Gossard, *Science* **309**, 2180 (2005).
- [36] T. Yu and J. Eberly, *Optics Communications* **264**, 393 (2006).
- [37] T. Yu and J. Eberly, *Physical review letters* **97**, 140403 (2006).
- [38] K. Ann and G. Jaeger, *Phys. Rev. A* **76**, 044101 (2007), URL <https://link.aps.org/doi/10.1103/PhysRevA.76.044101>.
- [39] T. Yu and J. H. Eberly, *Science* **323**, 598 (2009).
- [40] M. P. Almeida, F. de Melo, M. Hor-Meyll, A. Salles, S. Walborn, P. S. Ribeiro, and L. Davidovich, *science* **316**, 579 (2007).
- [41] F. Wang, P.-Y. Hou, Y.-Y. Huang, W.-G. Zhang, X.-L. Ouyang, X. Wang, X.-Z. Huang, H.-L. Zhang, L. He, X.-Y. Chang, et al., *Phys. Rev. B* **98**, 064306 (2018), URL <https://link.aps.org/doi/10.1103/PhysRevB.98.064306>.
- [42] S.-H. Chen, *Phys. Rev. B* **109**, 045308 (2024), URL <https://link.aps.org/doi/10.1103/PhysRevB.109.045308>.
- [43] S.-H. Chen, S. G. Tan, and C.-C. Huang, arXiv preprint arXiv:2410.04396 (2024).
- [44] A. Abliz, H. J. Gao, X. C. Xie, Y. S. Wu, and W. M. Liu, *Phys. Rev. A* **74**, 052105 (2006), URL <https://link.aps.org/doi/10.1103/PhysRevA.74.052105>.
- [45] G. Sadiq, E. I. Lashin, and M. S. Abdalla, *Physica B: Condensed Matter* **404**, 1719 (2009).
- [46] A. Mortezaipoor, M. A. Borji, and R. L. Franco, *Laser Physics Letters* **14**, 055201 (2017).
- [47] W. Dür, G. Vidal, and J. I. Cirac, *Phys. Rev. A* **62**, 062314 (2000), URL <https://link.aps.org/doi/10.1103/PhysRevA.62.062314>.
- [48] L. Theerthagiri and R. Ganesh, *Quantum Information Processing* **22**, 355 (2023).
- [49] A. Sharma and A. A. Tulapurkar, *Physical Review A* **103**, 052430 (2021).
- [50] A. Costa Jr and S. Bose, *Physical review letters* **87**, 277901 (2001).
- [51] S. Watanabe, *IBM Journal of research and development* **4**, 66 (1960).
- [52] A. Kumar, *Phys. Rev. A* **96**, 012332 (2017), URL <https://link.aps.org/doi/10.1103/PhysRevA.96.012332>.
- [53] M. Yamamoto, S. Takada, C. Bäuerle, K. Watanabe, A. D. Wieck, and S. Tarucha, *Nature Nanotechnology* **7**, 247 (2012).
- [54] D. Gunlycke, J. Jefferson, T. Rejec, A. Ramšak, D. Pettifor, and G. Briggs, *Journal of Physics: Condensed Matter* **18**, S851 (2006).